1995-12

Computation for a Three by Three Array of Protrusions Cooled by Liquid Immersion: Effect of Substrate Thermal Conductivity

Mukutmoni, D.; Joshi, Y.K.; Kelleher, M.D.

ASME

Mukutmoni, D., Y. K. Joshi, and M. D. Kelleher. "Computations for a three-by-three array of protrusions cooled by liquid immersion: Effect of substrate thermal conductivity." Journal of Electronic Packaging 117.4 (1995): 294-300.
http://hdl.handle.net/10945/62166

Computations for a Three-by-Three Array of Protrusions Cooled by Liquid Immersion: Effect of Substrate Thermal Conductivity

D. Mukutmoni
ADAPCO, Inc.,
Melville, NY 11747;
Currently, Cadillac/Luxury Car Division,
General Motors Corporation,
M/S 485-303-807,
Flint, MI 48557

Y. K. Joshi
Department of Mechanical Engineering and,
CALCE Electronics Packaging
Research Center,
University of Maryland,
College Park, MD 20742

M. D. Kelleher
Department of Mechanical Engineering,
Naval Postgraduate School,
Monterey, CA 93943

A computational study of natural convection in an enclosure as applied to applications in cooling of electronic components is reported. The investigation is for a configuration consisting of a three by three array of heated protrusions placed on a vertical substrate. The vertical sidewalls are all insulated, and the top and bottom walls serve as isothermal heat sinks. A thin layer at the back of each protrusion is the heat source, where heat is generated uniformly and volumetrically. The coolant is the flourinert liquid FC75. The code was first validated with experimental results reported earlier on the same configuration. The effect of the substrate conductivity, κ_s on the heat transfer and fluid flow was then studied for power levels of 0.1 and 0.7 Watts per protrusion. The computations indicate that the effect of increasing κ_s is dramatic. The protrusion temperatures which were found to be nominally steady, were substantially reduced. The percentage of generated power that is directly conducted to the substrate increased with an increase in κ_s. The fluid velocity field, which was unsteady, was not significantly affected by changes in κ_s.

Introduction

Due to higher densities and specific heats of liquids compared to air, significant enhancements in power dissipation rates from electronic components can be achieved during liquid immersion cooling. Candidate coolants for such applications must have high dielectric strength, be chemically inert, non-toxic and environmentally safe. A class of liquids called Fluorinerts has been developed (Product Manual, 3M Corporation, 1985) to specifically meet these requirements. Since the thermo-physical properties of these liquids are considerably different than those of conventional coolants such as water, their convective heat transfer characteristics are currently an active area of investigation. Both single phase, as well as phase change schemes are being studied, as described by Bar-Cohen and Bergles (1990) and Bar-Cohen (1991).

Single-phase liquid cooling studies have addressed both forced and natural convection. Many of the initial studies were experimental, typically investigating a particular geometrical configuration of discrete heat sources. Due to the multiplicity of geometric scales and thermo-physical properties involved in electronics cooling applications, their results are applicable only over relatively narrow parametric ranges. Computational investigations of liquid immersion cooling of discrete heat sources, including realistic effects such as three-dimensional transport (Liu et al., 1987; Wroblewski and Joshi, 1992) and conjugate processes (Joshi et al., 1991) have also been carried out.

Indeed, a combined computational and experimental approach appears to be best suited for the typically complex electronic cooling applications. The computational technique employed must first be validated over the range of flow vigor parameters investigated in the supporting experiments. This process provides important input on the appropriate grid sizes, as well as on the time step necessary to resolve the observed transport behavior. The latter is particularly important in high vigor natural convection flows, typical in many fluorinert liquids which have significantly higher volumetric expansion coefficients compared to water (Joshi et al., 1991). Following a detailed validation, the code may be used as a convenient tool by the thermal designer to study the effects of varying thermophysical properties and geometric parameters. The present study illustrates such approach.

Computations of liquid immersion natural convection cooling are presented for a three-by-three array of heat generating, substrate mounted, rectangular protrusions in an enclosure filled with dielectric liquid FC 75. The protrusions used in the present study simulate applications where: (i) package internal thermal resistance is a small fraction of its overall thermal resistance, (ii) packages are in intimate thermal contact with the substrate and (iii) additional thermal enhancements such as heat sinks are not provided at the package surfaces. The code is first validated with an experimental study of the same configuration. The effects of changing the substrate thermal conductivity are then investigated in detail. Due to the dielectric nature of FC 75, its thermal conductivity is almost an order of magnitude smaller than that of water. Consequently, the substrate plays a significant and sometimes dominant role in the heat removal from the protrusions.

The paper is organized in the following manner; the next section begins with a formulation of the problem. This is followed by comparison with previously reported experimental results. Effect of substrate thermal conductivity on fluid flow and heat transfer responses is next described. The paper ends with a summary of the major conclusions.

Formulation

Figure 1 shows the schematic of the configuration simulated in the present computations. This is the same model system examined experimentally by Joshi et al. (1991) for passive

Contributed by the Electrical and Electronic Packaging Division for publication in the JOURNAL OF ELECTRONIC PACKAGING. Manuscript received by the EEPD January 1, 1995; revised manuscript received July 19, 1995. Associate Technical Editor: B. G. Sammakia.

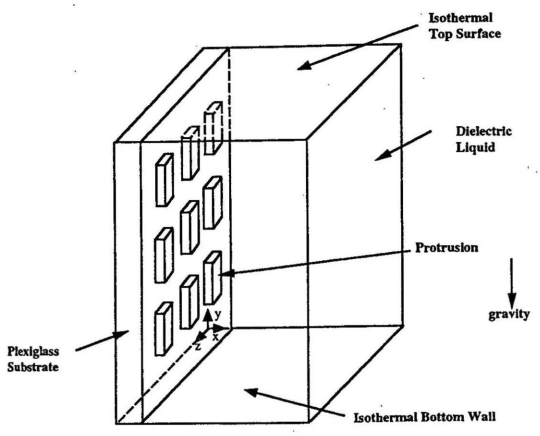

Fig. 1 Geometry of enclosure

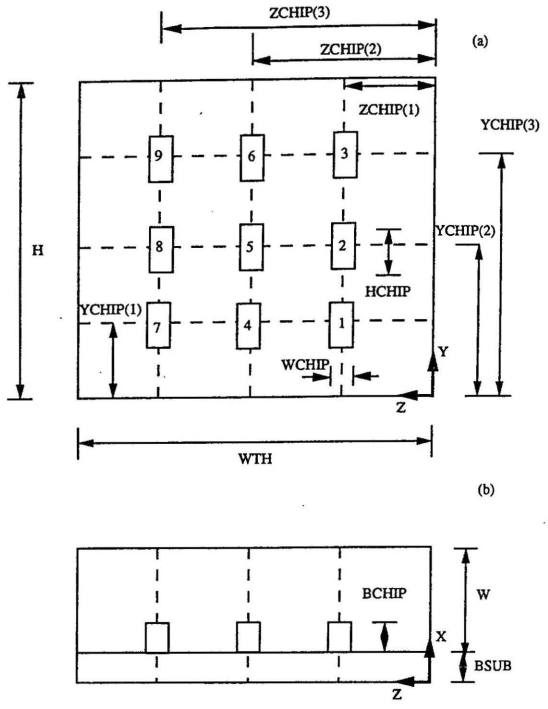

Fig. 2 Dimensions of the enclosure and protrusions, projected on (*a*) *Y-Z* plane and (*b*) *X-Z* plane

liquid immersion cooling. Detailed geometrical parameters are identified in figure 2. Table 1 gives a complete numerical listing of the geometric and thermo-physical parameters in the present study. The thermal conductivity ratio of the substrate and fluid is varied between 1 and 100, with all other parameters fixed. This range covers most of the commonly used substrates in applications. As indicated in Table 1, two different power dissipation levels were considered.

The nondimensionalized governing equations are:

$$\nabla \cdot \mathbf{U} = 0 \tag{1}$$

$$\frac{\partial u}{\partial t} + \nabla \cdot (u\mathbf{U}) = -\frac{\partial p}{\partial x} + \nabla \cdot (\mathrm{Pr} \nabla u) \tag{2}$$

$$\frac{\partial v}{\partial t} + \nabla \cdot (v\mathbf{U}) = -\frac{\partial p}{\partial y} + \nabla \cdot (\mathrm{Pr} \nabla v) + \mathrm{Bo}T \tag{3}$$

$$\frac{\partial w}{\partial t} + \nabla \cdot (w\mathbf{U}) = -\frac{\partial p}{\partial z} + \nabla \cdot (\mathrm{Pr} \nabla w) \tag{4}$$

$$\frac{\partial T}{\partial t} + \nabla \cdot (T\mathbf{U}) = \nabla^2 T. \tag{5}$$

In the above equations, the standard Boussinesq approximations are used with one exception. The viscosity of FC 75 is treated as temperature dependent. The substrate temperature is governed by:

$$\frac{R_s}{R}\frac{\partial T}{\partial t} = \frac{\kappa_s}{\kappa} \nabla^2 T. \tag{6}$$

The energy equation for each protrusion for most of its volume is

Nomenclature

A_x = BSUB + W/H , aspect ratio in the x-direction
A_z = WTH/H , aspect ratio in the z-direction
BCHIP = size of protrusion in x-direction, m
Bo = $gq\beta L^5/\alpha^2 k_c$, Boussinesq number
BSUB = thickness of substrate, m
C = specific heat, J/kg K
g = acceleration due to gravity, m/s^2
H = height of the cavity, m
HCHIP = size of protrusion in y-direction, m
Nu = Nusselt number at the protrusion faces
$\mathrm{Nu}_{\mathrm{avg}}$ = average Nusselt number at the faces
p = nondimensional pressure
Pr = ν/α , Prandtl number
q = volumetric heat generation rate, W/m^3
Q = power dissipated per protrusion, W
R = product of density and specific heat, J/m^3 K
T = nondimensional temperature
t = nondimensional time
T_{wall} = temperature of horizontal walls, °C
$\mathbf{U}$ = nondimensional velocity vector
W = width of enclosure in x-direction minus the substrate, m
WCHIP = size of protrusion in z-direction, m
WTH = dimensions of enclosure in z-direction, m
X, Y, Z = dimensional spatial coordinates, m
x, y, z = nondimensional spatial coordinates, scaled by H
YCHIP(1), . . . = location of protrusion centers in y-direction, m
ZCHIP(1), . . . = location of protrusion centers in z-direction, m
α = thermal diffusivity, m^2/s
β = coefficient of volume expansion, 1/K
κ = thermal conductivity, W/mK
ν = dynamic viscosity, m^2/s
ρ = density, kg/m^3

Subscripts

c = protrusion
s = substrate
x = x-direction
z = z-direction

Table 1 List of the parameters prescribed for the problem. Units are given in Nomenclature.

Parameter	Value	Parameter	Value
WTH	0.2032	H	0.152
W	0.030	BSUB	0.0195
HCHIP	0.024	WCHIP	0.008
BCHIP	0.006	YCHIP (1)	0.038
YCHIP (2)	0.076	YCHIP (3)	0.114
ZHIP (1)	0.0508	ZCHIP (2)	0.1016
ZCHIP (3)	0.1524	Q	0.1, 0.7
T_{wall}	10.0		
κ_c/κ	3732.0	κ_s/κ	A variable
R_c/R	1.2	R_s/R	0.262
κ	0.064		

$$\frac{R_c}{R}\frac{\partial T}{\partial t} = \frac{\kappa_c}{\kappa}\nabla^2 T. \tag{7}$$

The volumetric heat source is restricted to a layer in the protrusion that is one control volume thick in the x-direction, immediately next to the substrate. This simulates the heating of the protrusions at their bases by thermofoil heaters in the experiments by Joshi et al. (1991). The thickness of this layer for the present computations is 0.5 mm. The energy equation for this layer is

$$\frac{R_c}{R}\frac{\partial T}{\partial t} = \frac{\kappa_c}{\kappa}(\nabla^2 T + 1). \tag{8}$$

In the above equations, the non-dimensional spatial coordinates x, y, and z were obtained from the dimensional coordinates X, Y, Z by scaling with H, the enclosure height, the velocities were scaled by α/H, the time by H^2/α and the difference between the total pressure and the equilibrium hydrostatic pressure in the absence of a temperature gradient was scaled by $\rho\alpha^2/H^2$. The temperature was non-dimensionalized by first subtracting T_{wall} and then dividing by qH^2/κ_c, the temperature scale, where T_{wall} is the temperature of the top and bottom walls. Also, κ_c and κ_s are the thermal conductivities of the chip and substrate respectively and R_c and R_s are the respective products of the density and specific heat for the protrusion and substrate. Also, note that Pr, the Prandtl number, is a function of the temperature and hence the spatial coordinates. Bo the Boussinesq number, is the product of the Rayleigh number and the Prandtl number.

The boundary conditions consistent with the adiabatic side walls (including the back of the substrate) and isothermal top and bottom walls in a nondimensional form are the following:

$$x = 0, A_x; \quad 0 \le z \le A_z, \quad 0 \le y \le 1$$

$$u = v = w = 0 \quad \frac{\partial T}{\partial x} = 0 \tag{9}$$

$$z = 0, A_z; \quad 0 \le x \le A_x; \quad 0 \le y \le 1$$

$$u = v = w = 0 \quad \frac{\partial T}{\partial z} = 0 \tag{10}$$

$$y = 0, 1; \quad 0 \le x \le A_x; \quad 0 \le z \le A_z;$$

$$u = v = w = 0 \quad T = 0. \tag{11}$$

From the governing equations and boundary conditions, four additional parameters are found, namely the thermal conductivity ratios and density-specific heat product ratios of the protrusion-fluid and the substrate-fluid combinations. The property parameter values used in this study, provided in Table 1, are chosen to match the experiments of Joshi et al. (1991). The temperature dependent viscosity (Prandtl number in the non-dimensional formulation) for FC75 has been taken from a curve fit to the properties data as in Joshi et al. (1991):

$$\Pr(T_d) = 29.088(1.4074 - 2.96 \times 10^{-2} T_d + 3.8018 \times 10^{-4} T_d^2 - 2.7316 \times 10^{-6} T_d^3 + 8.168 \times 10^{-9} T_d^4). \tag{12}$$

The temperature T_d in Eq. (12) is dimensional and in degree Celcius. For high power levels when the temperature rise in the protrusions are in the order of tens of degrees, the Prandtl number can vary by a factor of 2.

The governing equations were solved in primitive variables on a three-dimensional staggered grid, based on the finite volume method (Patankar, 1980). The QUICK scheme (Leonard, 1983) and the SIMPLEX algorithm (Van Doormal and Raithby, 1984) were used to solve these. The time step was chosen such that the maximum Courant number $u\Delta t/\Delta x$ (where Δt and Δx are the time step and grid size, respectively) was maintained less than 1.0. The time-stepping was achieved by a first order backward Euler scheme.

Non-uniform grids are required for this problem since the flow field has boundary layer type of behavior near the wall, along the substrate and protrusions. The grid used in the calculation is shown in Fig. 3. A $30 \times 36 \times 66$ nonuniform grid was used for the calculations. Extra resolution is provided near the boundary layer regions. Further implementation details are provided in Mukutmoni et al. (1993).

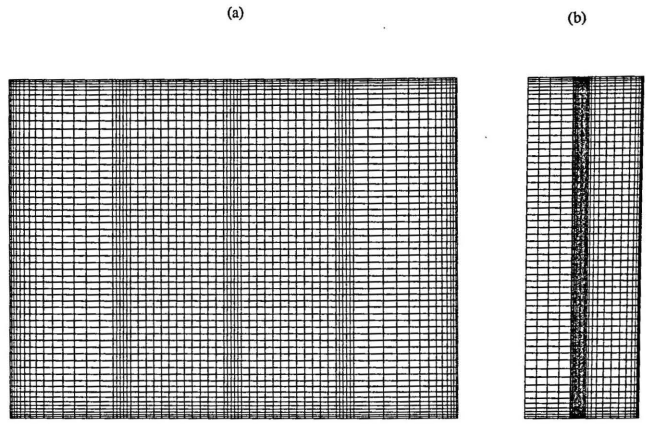

Fig. 3 Computational grid (*a*) *y-z* plane (*b*) *x-y* plane

Validation and Grid Refinement Studies

The results of the calculations were compared with some of the experimental results of Joshi et al. (1991) for $Q = 0.1$ W and $Q = 0.7$ W per protrusion. The protrusion temperatures were calculated by taking a volume average of the control volume temperatures contained in the protrusions. The average protrusion temperatures of the bottom and top rows have been compared in Table 2 and show good agreement. The same qualitative features are also maintained within the protrusion

Table 2 Comparison between protrusion temperatures (°C) of experiments (Joshi et al., 1991) (referred to as Exp.) and present study (referred to as Num.) for power levels of 0.1 W and 0.7 W. The conductivity ratio between substrate and fluid is unity.

Component number	$Q = 0.1$ W Num.	Exp.	$Q = 0.7$ W Num.	Exp.
Top row average	13.1	13.1	26.2	N/A
Bottom row average	12.9	12.8	24.8	21.6

array. In both the computations and experiments, the bottom row of protrusions are relatively cooler than the top row. The better agreement for the lower power level (Table 2) is because in the numerical model the side walls were assumed to be adiabatic. In reality, as the protrusion temperatures rise, the heat loss through the side walls is no longer negligible. These heat losses were not monitored in the experiments, making it difficult to incorporate them in the numerical model.

The results given in Table 2 are an end result of a large volume of computations with various nonuniform grid sizes. Basically, the grid sizes were decreased until the protrusion temperatures were sufficiently close to the experiments. Various other parameters were also adjusted such as resolution near the protrusions and the sizes of the control volumes next to the wall. The comparison with experiments also indicates the essential correctness and accuracy of the code, as well as the adequacy of the grid resolution. The code has also been fully validated for other enclosure flows. Further details are given in Mukutmoni et al. (1993).

Effect of Substrate Conductivity

With the validated code, the effect of varying κ_s was investigated with all geometric dimensions and thermo-physical parameters fixed. Two different power levels were looked into, namely 0.1 W and 0.7 W of power dissipation per protrusion. The resulting velocity and temperature fields for all substrate thermal conductivities were unsteady. However, the temperatures within the protrusions and the substrate were found to be relatively steady, due to the disturbance dampening effect of the solid regions. Overall, it was found that the substrate thermal conductivity significantly affects the heat transfer from the protrusions. The flow field is affected less profoundly. We now examine these features in more detail.

Temperature Field. The average protrusion temperature rise as a function of κ_s/κ is shown Fig. 4(a). As κ_s/κ is increased from 1 to 100, the average protrusion temperatures are reduced by almost 50 percent. Similarly, for the same conductivity ratio range, the percentage of heat going into the substrate directly from the protrusions is increased significantly. At a conductivity ratio of unity, barely 5% of the generated power is being conducted directly into the substrate (Fig. 4(b)). This

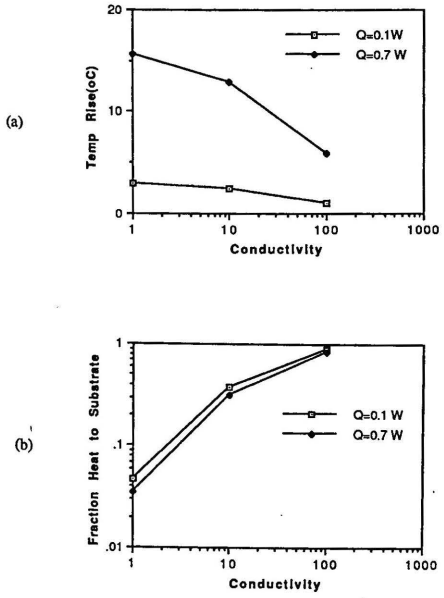

Fig. 4 The effect of substrate to fluid thermal conductivity ratio on (a) the average protrusion temperature rise, (b) the fraction of net heat generated that is conducted to the substrate

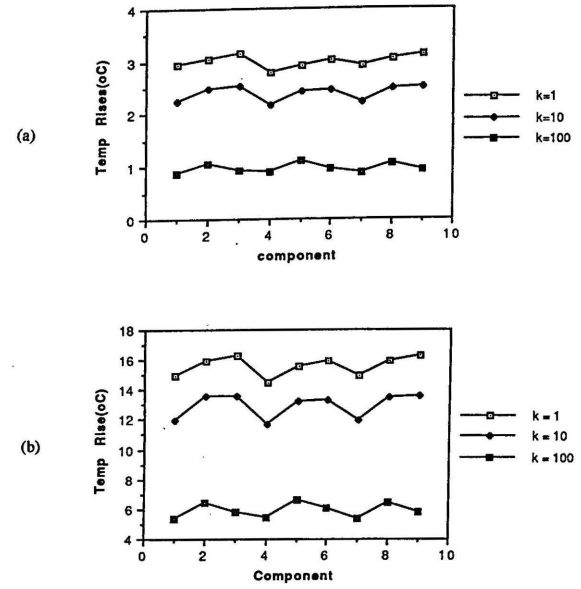

Fig. 5 The temperature rise of individual protrusions for different substrate to fluid thermal conductivity ratios; (a) Q = 0.1 W, (b) Q = 0.7 W. The component numbers are as shown in Fig. 2(a).

demonstrates the relative dominance of the convection process. At a conductivity ratio of 100, typical of a ceramic substrate in a fluorocarbon liquid, almost 90 percent of the generated power is going directly into the substrate, prior to being convected into the fluid.

A high thermal conductivity substrate acts as a heat sink, reducing the protrusion temperatures. Heat conducted from the protrusions to the substrate is also efficiently transferred to the top and bottom enclosure walls. For the same substrate conductivity, the fraction of heat transferred to the substrate is slightly lower at the higher Q (Fig. 4(b)). This is a reflection of the fact that convection is relatively stronger for higher Q's.

The temperatures of the individual protrusions are shown in Fig. 5 for Q = 0.1 and 0.7 W. The component numbers are indicated in Fig. 2(a). The temperatures of the components for different thermal conductivity ratios for Q = 0.1 W are shown in Fig. 5(a). It is seen that a rough vertical symmetry is maintained. The component temperatures in the left column (7, 8 and 9) are roughly the same as the right column temperatures (1, 2 and 3).

For all cases, the coolest temperatures are located at the bottom row. And the coolest component number is always 4 (bottom row, middle column). It is interesting to note that the hottest row is the top one, for the lower conductivities. For the highest conductivity, it is the middle row that is the warmest (Fig. 5(a)). The results for Q = 0.7 W are qualitatively similar (Fig. 5(b)). The component temperatures are, as expected, higher.

Figure 6 shows the fraction of heat loss to the substrate for individual components. The fraction of heat loss to the substrate was found to be maximum for the components of the bottom row. The only exception is for a conductivity ratio of 100, for which it is the top row components whose fraction of heat to the substrate is highest. This is consistent with the protrusion temperature results. It was found that as κ_s is increased, the top row components get relatively cooler. This trend is observed both for Q = 0.1 (Fig. 6(a)) and for Q = 0.7 (Fig. 6(b)).

Figure 7(a) shows the variation of the average Nusselt numbers with the substrate thermal conductivity for the different protrusion faces for a power dissipation level of 0.1 W per protrusion. Four cases are reported; top and bottom (in the y-direction), front (in the x-direction) and the average of the sides (in the z-direction). The local Nusselt number was calculated

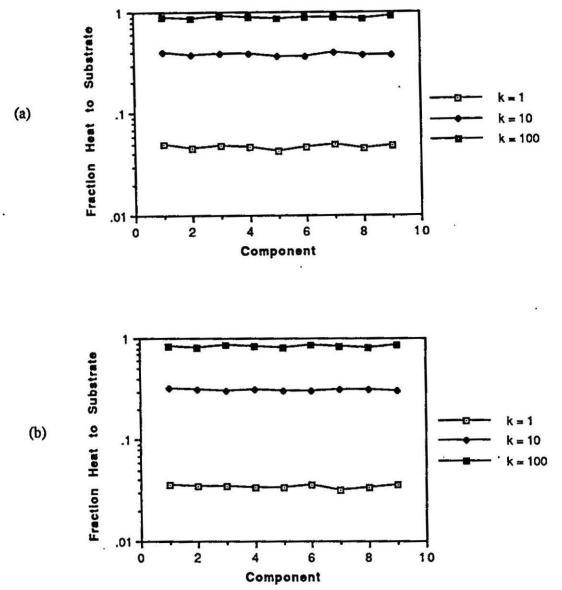

Fig. 6 The fraction of net generated power, conducted to the substrate for individual protrusions for different substrate to fluid thermal conductivity ratios; (*a*) Q = 0.1 W, (*b*) Q = 0.7 W

by a numerical implementation of the following at the fluid-protrusion interfaces:

$$\mathrm{Nu} = \frac{1}{T}\frac{\partial T}{\partial x} \tag{13}$$

The average Nusselt numbers reported in Fig. 7(*a*) were calculated by numerically integrating over each surface and for all the nine protrusions, i.e.,

$$\mathrm{Nu}_{\mathrm{avg}} = \frac{\int \mathrm{Nu}\,\mathbf{dS}}{S} \tag{14}$$

Nu values are particularly useful if calculations are to be done for the conduction region alone, without solving a conjugate

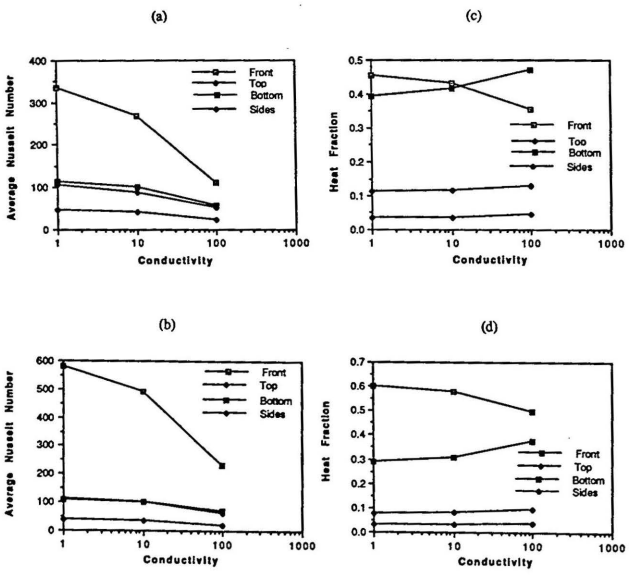

Fig. 7 Effect of κ_s/κ on average Nusselt number for all components for different faces for (*a*) Q = 0.1 W, (*b*) Q = 0.7 W, and on fraction of net generated power convected to the fluid from various faces for (*c*) Q = 0.1 W, (*d*) Q = 0.7 W

Table 3 Average Nusselt numbers for individual components for Q = 0.7 W and κ_s/κ = 100

Component number	Front face	Top face	Bottom face	Side faces
1.	251.5	57.8	76.9	19.6
2.	249.1	66.4	69.9	19.3
3.	202.4	62.2	57.4	16.5
4.	252.1	59.3	77.4	26.0
5.	243.9	67.0	71.6	26.0
6.	206.6	66.3	58.9	22.3
7.	249.7	58.0	77.0	20.2
8.	253.8	66.0	69.7	20.0
9.	192.1	66.5	57.3	17.2

domain problem. In such a case, the convection domain will be replaced by convection coefficients estimated from the Nusselt numbers. It is noted that the Nusselt numbers reported here are based on the height of the enclosure.

It is seen from Fig. 7(*a*) that as the substrate thermal conductivity increases, the average Nusselt numbers decrease, most dramatically for the front face. The top and bottom faces and the sides are less affected by the substrate conductivity. The drop in Nusselt number is expected in light of Fig. 6, which shows that a larger percentage of generated heat goes to the substrate directly, when the substrate thermal conductivity is increased. The least affected are the side faces. Figure 7(*b*) shows the average Nusselt numbers of the faces for a power dissipation level of 0.7 W per protrusion. The same trends are repeated, except that the Nusselt number values are higher. This is a mere confirmation of the fact that at higher power levels, the flow is more convectively dominated and more heat is transferred directly to the fluid, rather than first through the substrate.

In Table 3, the average Nusselt numbers for the individual protrusion components for a specific case are collected. The variation between protrusions is not significant and the changes are only around 10 percent about the mean (Table 2). This justifies the use of average values over all protrusions, as presented in Fig. 7(*a*) and (*b*).

In Fig. 7(*c*), the fraction of the generated heat, leaving each surface orientation is shown as a function of the substrate thermal conductivity ratio, for a power level of 0.1 W. This fraction is the ratio of heat transferred from a particular face orientation to the total heat transferred to the fluid, directly from the protrusions. One surprising result is the relatively high fraction of heat that leaves the bottom face, being of the same order as the front face loss. Together, the front and bottom faces account for greater than 80 percent of the net heat loss. We see that the fraction of heat leaving the front face decreases and the fraction from the bottom face increases with relatively small changes in the top and side faces, as the substrate conductivity is increased. The corresponding fractions at a power level of 0.7 W, in Fig. 7(*d*), show numerical values different from Fig. 7(*c*), but the same general trends. One important exception is that the front face yields the highest fraction over the entire range of thermal conductivities of the substrate.

Fig. 8(*a*) plots the dimensional temperature contours in the z-y plane at the fluid-substrate and protrusion-substrate interface. The power level is 0.7 W per protrusion and the substrate conductivity ratio is unity. The contour intervals are uniform. So, a crowding of isotherms implies sharper gradients, seen for example at the substrate-protrusion boundaries and at the top and bottom walls (Fig. 8(*a*)). At the same power level, but higher conductivity ratio (Fig. 8(*b*)), one observes more evenly spaced isotherms in the substrate. This is to be anticipated, since as the conductivity increases, a lower temperature gradient is required to transport the heat by conduction.

The local Nusselt numbers calculated using Eq. (13) are seen in Fig. 9 as equally spaced contours, for all faces and all nine components, for Q = 0.7 W and κ_s/κ = 1. The contour plots for

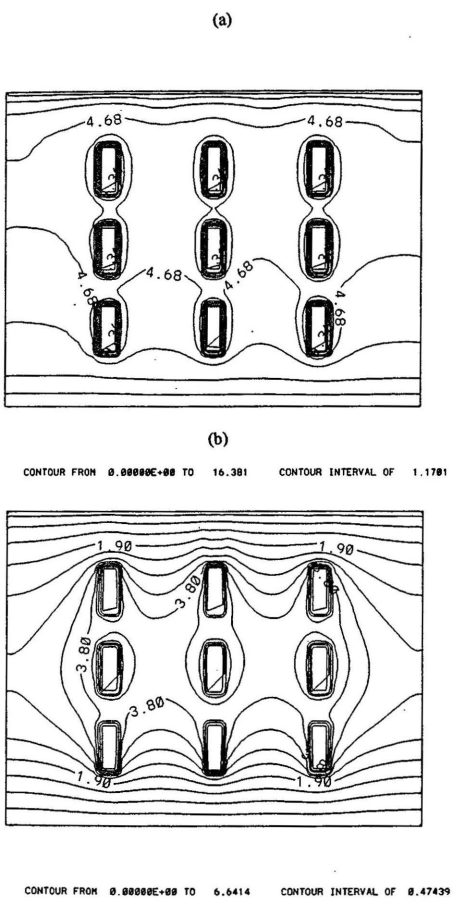

Fig. 8 Dimensional temperature contours in the Z-Y plane for X = 0.0195 m and Q = 0.7 W. (a) κ_s/κ = 1.0 (b) κ_s/κ = 100

the various components correspond to their physical locations in Fig. 2. All plots are also in the respective coordinate plane in the positive sense. For the front face, one observes evidence of vertical flow stratification, with the Nusselt numbers decreasing downstream for all the components. Thus, more heat is transferred at the lower regions of the front faces. On the side faces, one observes a similar vertical stratification. However, there is a boundary layer behavior in the heat generating layer next to the substrate. The Nusselt number variation is the least among the top and bottom faces, except for a crowding of contours in the heat generating region of the protrusions, similar to what was observed for the side faces.

Velocity Field. The fluid velocity field in the enclosure is considerably complicated. While the temperature field within the solid regions was nominally steady, the fluid velocity field was highly unsteady in certain regions. This field was looked into with the help of particle pathlines, as shown in Fig. 10(a) for κ_s/κ = 100 and Q = 0.7 W. The particle pathlines are in the z-y plane at a distance of 0.5 mm from the front faces of the protrusions. The pathlines were calculated by integrating the velocity field, assuming steady conditions. The results will match experimental flow visualization techniques (using aluminum particles in an illuminated sheet, for instance) if the flow field is steady or changes slowly in the exposure period.

Figure 10(b) shows the pathlines for the same section at a different instant. One observes that the main features of the flow such as quiescence at the bottom and the vertical plumes along the front faces are relatively unchanged. However, the region between the vertical plumes in Figs. 10(a) and 10(b) is highly vortical, changing significantly with time. The overall stability of the main features of the flow may be one reason why the component temperatures are effectively time-independent.

Figure 10(c) and 10(d) show the pathlines in the z-y plane near the wall opposite to the front faces. The flow descends along the plane and no plume like structures are observed. However, rapidly changing vortices (Figs. 10(c) and (d)) are seen, even in this plane, which is only 0.5 mm from the wall. The unsteady nature of the flow is further emphasized in Fig. 10(e), where the u-velocity at (0.190, 0.700, 0.894) is plotted as a function of the nondimensional time. It is clear that an unsteady formulation is necessary to capture the details of the flow patterns.

Summary and Conclusions

The flow and heat transfer characteristics were numerically investigated for a three by three array of protrusions mounted on a vertical substrate that is being cooled by the dielectric liquid FC75 in an enclosure. The computations are in good agreement with measured protrusion temperature rises for a power dissipation level of 0.1 W and 0.7 W. The effect of varying the substrate thermal conductivity was investigated in detail. The results indicate that component temperatures decrease significantly as the conductivity is increased. Also, the percentage of heat going directly into the substrate from the protrusions increased. It was found that most of the heat rejected from the components came from the front and bottom faces. Also, the local Nusselt numbers at the faces supported a trend of vertically stratified flow. More heat was rejected from the lower portions.

The temperature field both in the substrate and the protrusions was nominally steady for both power levels considered. The components in the bottom row were found to be the coolest. The temperature field had sharp gradients at the top of the substrate-fluid interface for substrates of low thermal conductivity. The velocity field showed marked unsteadiness, although the main features such as the vertical plumes along the protrusions changed very little. The bottom region of the enclosure was found to be relatively stagnant.

The present study clearly demonstrates the need for a combined experimental and computational approach for the thermal design of electronic systems. The complexities in geometry and

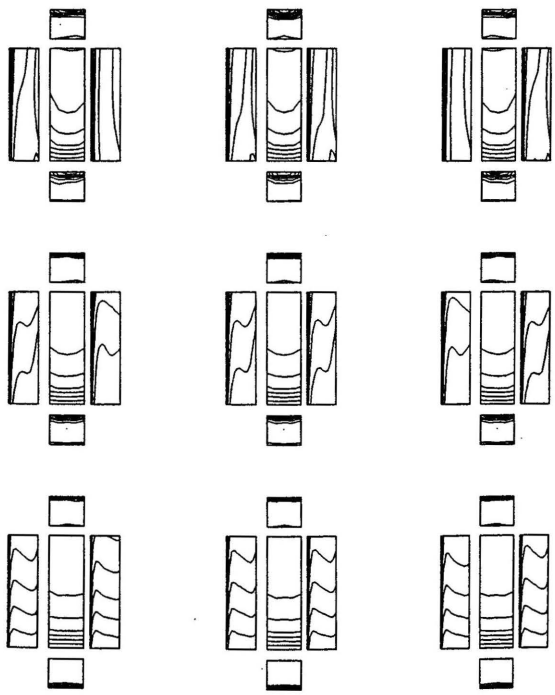

Fig. 9 Local Nusselt number contours on various faces of all components for Q = 0.7 W, κ_s/κ = 1

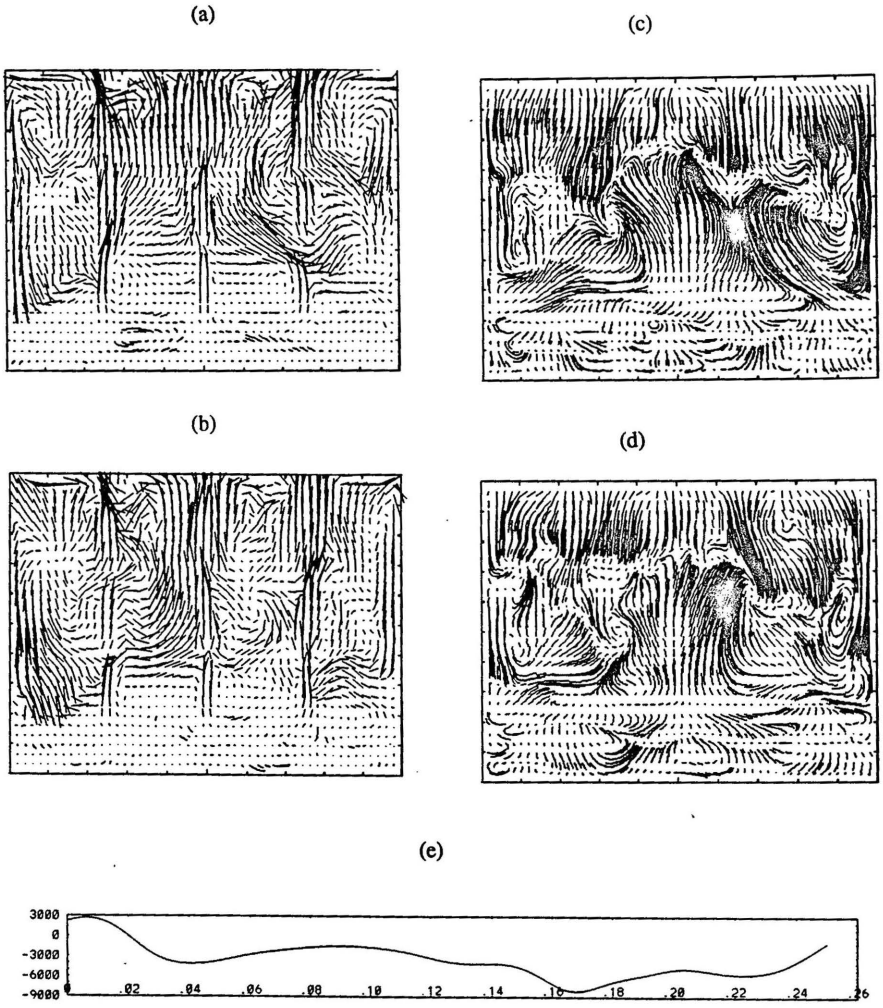

Fig. 10 Particle pathlines for Q = 0.7 W and κ_s/κ = 100 in the Z-Y plane at X = 0.026 m at (*a*) t = 0, (*b*) t = 0.25, and X = 0.049 m at, (*c*) t = 0, and (*d*) t = 0.25. Also shown is the timewise variation in u-velocity, (*e*), at the non-dimensional location of x = 0.190, y = 0.700 and z = 0.894.

heat dissipation patterns, along with the unique fluid thermophysical properties examined in this study result in large unsteadiness in the flow field. In order to achieve a predictive capability for design, it is essential that the numerical parameters such as grid sizes and time steps be refined by comparisons against experiments.

Acknowledgments

The support from the Naval Surface Warfare Center, Crane, IN through the SHARP effort is gratefully acknowledged. This study was performed when all authors were at the Naval Postgraduate School. The computations were carried out on a Cray Y-MP/EL 4/1024 of the Naval Postgraduate School.

References

Bar-Cohen, A., 1991, "Thermal Management of Electronic Components With Dielectric Liquids," *Proc. ASME/JSME Thermal Engineering Joint Conference,* Vol. 2, pp. xv-xxxix.

Bergles, A. E., and Bar-Cohen, A., 1990, *Direct Liquid Cooling of Microelectronic Components, Advances in Thermal Modeling of Electronic Components and Systems,* Vol. 2, A. Bar-Cohen and A. D. Kraus, eds., ASME Press, pp. 233–342.

Joshi, Y. K., Kelleher, M. D., Powell, M., and Torres, E. I., 1991, "Natural Convection Heat Transfer from an Array of Rectangular Protrusions in an Enclosure filled with Dielectric Fluid," ASME HTD-Vol. 183, pp. 9–18.

Leonard, B. P., 1983, "A Convectively Stable, Third-Order Accurate Finite-Difference Method for Steady Two-Dimensional Flow and Heat Transfer," *Numerical Properties and Methodologies in Heat Transfer,* Shih, T. M., ed., Hemisphere Publishing, Washington, D.C., pp. 211–226.

Liu, K. V., Yang, K. T., and Kelleher, M. D., 1987, "Three-Dimensional Natural Convection Cooling of an Array of Heated Protrusions in an Enclosure Filled with a Dielectric Liquid," *Proc. Int. Symp. on Cooling Technology for Electronic Equipment,* Honolulu, Hawaii, pp. 486–497.

Mukutmoni, D., Kelleher, M. D., and Joshi, Y. K., 1993, "AMPHIB: A Users Manual," Technical Report NPS-ME-93-001, Naval Postgraduate School, Monterey, CA.

Patankar, S. V., 1980, *Numerical Heat Transfer and Fluid Flow,* Hemisphere, McGraw-Hill, New York.

Product Manual, Fluorinert Liquids, 1985, 3M Corporation, Minneapolis, MN.

Van Doormaal, J. P., and Raithby, G. D., 1984, "Enhancements of the Simple Method for Predicting Incompressible Fluid Flows," *Numerical Heat Transfer,* Vol. 17, pp. 147–163.

Wroblewski, D. E., and Joshi, Y. K., 1992, "Transient Natural Convection from a Leadless Chip Carrier in a Liquid Filled Enclosure: A Numerical Study," ASME JOURNAL OF ELECTRONIC PACKAGING, Vol. 114, pp. 271–279.